Influence of Joint Conformity on the Failure Mechanisms of the Glenoid Implant – a finite element analysis

Maria do Carmo Rocha e Melo Belard Raimundo

maria.belard.raimundo@tecnico.ulisboa.pt

Instituto Superior Técnico, Universidade de Lisboa, Portugal

October 2021

Glenoid loosening is the most common complication after anatomic total shoulder arthroplasty, making up 80% of long term complications. Several mechanisms lead to glenoid loosening, including the failure of the implant itself (wear or fracture), lack of support of the underlying bone and inadequate fixation. The glenoid implant has suffered many alterations in composition and design over the years and their influence on joint and implant stability has been studied. However, the understanding of the influence of articular conformity in glenoid loosening is still limited. This study aimed to understand whether the conformity of the joint influences the failure of the glenoid component. Therefore, finite element analyses of three articular configurations of 1mm, 3mm and 5mm radial mismatch, were performed. The joint reaction forces obtained using a multibody model of the upper limb for abduction and flexion movements in different degrees of motion were applied in the FE model. To assess the influence of joint conformity in the mechanisms of glenoid loosening three analyses were performed. Firstly, the humeral translations retrieved from the multibody model were analyzed for the different configurations. Secondly, the evaluation of the Von Mises stresses on the cement allowed for the analysis of the mechanical failure of the material under cyclic loading. Finally, to analyze the bone-cement interface, the Hoffman failure criteria was applied, using both normal and shear stresses on the interface. The results showed that the more conforming configuration has lower risks of failure under healthy physiological conditions when compared to less conforming designs.

Keywords: Anatomic total shoulder arthroplasty, Glenoid loosening, Failure mechanisms, Finite element analysis.

1. Introduction

The Anatomic Total Shoulder Arthroplasty (TSA) is a surgical procedure that replaces the damaged joint with a prosthesis that recreates the anatomy and function of the normal shoulder. With a polyethylene glenoid and a cobalt-chromium humeral head, the anatomic TSA is considered standard treatment for glenohumeral osteoarthritis (GHOA). The use of TSA has increased in the last two decades as the advance in prosthesis design and type has allowed its use in an increasing number of indications.

Regardless of its evolution over the years, the TSA outcomes are still far from perfect with a complication rate of 10.3% [1].The most common complications include loosening of the components, periprosthetic fractures, glenoid wear, rotator cuff tears, joint instability, neurologic injuries and infection. In 2017, Bohsali et al. [1] reviewed all complications of anatomic TSA reported in studies from 2006 to 2015, stating that component loosening following TSA made up 39% of the post-surgical complications, with approximately 38% corresponding to glenoid loosening and only 1% corresponding to humeral component loosening. Moreover, the second highest incidence rate was for glenoid wear, which corresponded to 22.6% of all complications, followed by shoulder instability, with an incidence of 10.1%.

Glenoid loosening accounts for the largest share of unsatisfactory results after the procedure and is clinically related to arthralgia and function impairment [2]–[5].

The failure mechanisms of the glenoid include failure of the component itself, which can happen due to fracture of the implant or changes in the implant surface, usually linked to wear of the

polyethylene [6], [7]. Furthermore, the glenoid implant can fail due to lack of support of the underlying bone, inadequate initial fixation, or through a phenomenon called rocking-horse effect.

Over the years, FE analysis has provided insight into the influence of implant design features on the joint stability, especially on the major clinical issue of glenoid loosening. The design parameters covered in the literature include implant geometry and material, orientation and positioning of the components and fixation methods (cement/uncemented glenoid fixation) .

However, the understanding of the influence of glenohumeral conformity in the loosening of the glenoid component is scarce.

Although a few studies acknowledge this topic, the optimal radial mismatch between the glenoid and humeral head components is yet to be determined since conforming designs allow for greater stability but also carry the risk of eccentric loading in the course of humeral translation over the glenoid. Besides, the presence of a mismatch allows for the humerus to translate at the expense of reducing contact area, increasing the possibility of polyethylene failure due to increased contact stresses.

Despite the contribution of previous studies to the body of knowledge, most of them are clinical and mechanical studies and finite element models studying this topic are scarce. Therefore, this study presents a finite element analysis of three different TSA configurations to expand the knowledge on the influence of articular conformity in the loosening mechanisms of the glenoid implant.

2. Materials and Methods

The methodology of this study included the modulation of the TSA components – glenoid implant, cement and humeral head – , the virtual implantation of the components on the bone and the finite element modeling of the TSA.

2.1. Geometric modeling of the TSA

The glenohumeral joint model, used in this study, was provided by the research group in which the project was developed [8], [9]. It corresponds to the right shoulder of a male and was obtained through the computational processing of CT data.

The modeling of the other components of the TSA was performed using SolidWorks and was based on the Global Anchor Peg Glenoid Shoulder System by DePuy. This system is divided into two components, the glenoid and the humeral head.

Glenoid component

The glenoid component used in this study was a 4 pegged, convex back, all-PE implant and was modelled according to the dimensions in Table 1.

The dimensions were chosen according to the properties of the studied GH joint. To study different mismatch configurations, the glenoid was left unchanged, while the humeral head radius was changed [10]. The radius of the glenoid implant was chosen according to the same catalog, and adapted to the size of the glenoid in study, being fixed at 27mm.

Table 2.1: Glenoid dimensions used for modeling [11].

Height	*39.4mm*
Width	28.9mm
Depth	6mm
Central peg length	15.2mm
Peripheral peg length	6.4mm
Peg diameter	5mm

The reaming of the glenoid was made with the help of a guide pin and a spherical reamer with the same radius as that of the glenoid implant. Over reaming of the glenoid cavity of the scapula was avoided in order to maximize the bone stock preservation for proper implant fixation. For glenoid fixation, a cement mantle of 1mm [12] was modelled. The cement did not cover the central peg as this is an anchor peg covered in a bone paste from the bone retrieved during glenoid preparation. This helps facilitate tissue integration, improving implant fixation and, consequently, its survival time.

Humeral component

Three humeral components were modelled to define three radial mismatches. The radii used were 26mm, 24mm and 22mm to obtain mismatches of 1, 3 and 5 millimeters, respectively. The implant was designed as a cut semi sphere with 18mm of height according with the specifications in the DePuy surgical technique catalog. For the sake of simplicity, as it did not affect the aim of this study, the stem of the humeral components was neglected.

For the implantation of the humeral component, the humerus was cut according with a humeral head cutting guide (fixed at 135º) to mimic the humeral resection described in the surgical technique catalog [13].

The final model was achieved by assembling all components. The different mismatches were applied only in the humeral head diameter as the rest of the model remained unchanged. The final configurations were approved by an orthopedic surgeon (Dr. Marco Sarmento from Hospital of Santa Maria, Faculty of Medicine, University of Lisbon) and are depicted in Figure 2.1 and Figure 2.2.

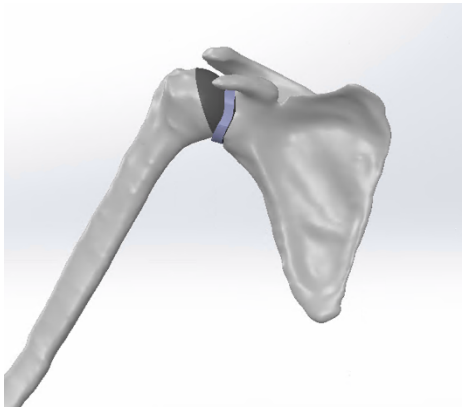

Figure 2.1: TSA model for 3mm mismatch.

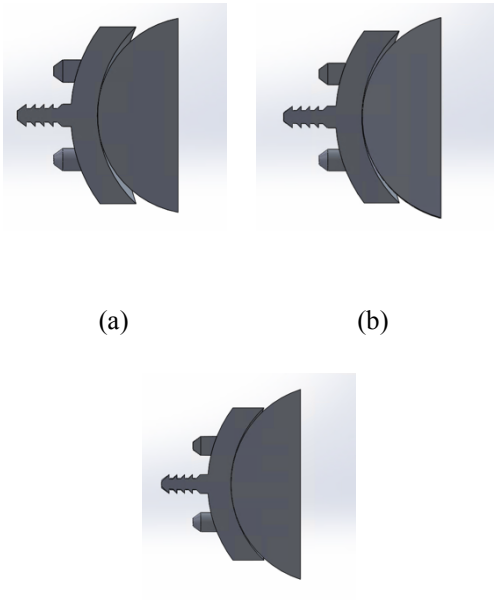

(a) (b)

(c)

Figure 2.2: GH configurations for three TSA. (a) 5mm radial mismatch; (b) 3mm radial mismatch; (c) 1mm radial mismatch.

2.2. Finite element modeling of TSA

Three finite element models were developed in Abaqus, one for each radial mismatch configuration. In Abaqus, the humeral component was simplified into an analytical rigid sphere.

Material properties

The components of the implant were assigned isotropic materials with a linear and elastic behavior. Their mechanical properties were defined according with the materials specified in the DePuy surgical technique catalog—the glenoid component, bone cement, and humeral head are composed of polyethylene (UHMWPE), Poly(methyl methacrylate) (PMMA), a cobalt-chromium alloy, respectively [14]. The mechanical properties considered are summarized in Table 2.2. Because the humeral head was modeled as a rigid analytical surface, no material properties needed to be defined

Table 2.2: Material properties for the glenoid implant and bone cement.

Material	*Young's modulus*	*Poisson's ratio*
UHMWPE	500 MPa	0.4
PMMA	2000 MPa	0.23

The properties of the scapula, however, depend on bone density. Considering a Poisson's ratio of 0.3 for bone, the Young's modulus was defined using the relationship between elasticity and bone density proposed by Gupta et. al. [15], given by:

$$E = 1049.5 \times 10^{-6}\rho^2, \ \ \rho \geq 350\ kg.m^3 \quad (2.1)$$

$$E = 3 \times 10^{-6}\rho^3, \ \ 350 < \rho \leq 1800\ kg.m^3 \quad (2.2)$$

where ρ is bone apparent density. The data from the research group also included bone densities for the scapula, estimated from the CT data using a relationship between Hounsfield units and bone density, a mapping procedure developed by the research group was applied to map the bone densities from the original geometry to the meshes of the TSA configurations. At the external surface of the scapula, all nodes were assigned maximum bone density, $1.86 g/cm^3$.

Meshing

The FE meshes were created individually for each component. For both the cement and glenoid component, excluding the central peg, linear hexahedral (C3D8) elements were used. The scapula and central peg of the glenoid component were meshed using quadratic tetrahedral (C3D10) elements. The size of the elements to be used was defined after a convergence analysis on the maximum contact pressure of different interfaces. The average element size selected for the bone cement and glenoid component was 0.5mm. The scapula's mesh was divided into two sections, each with its own element size: the section surrounding the glenoid cavity, was assigned 1mm elements due to its expected relevance in the analysis of the failure mechanisms of glenoid loosening, the more medialized area was assigned 2mm elements

Table 2.3: Mesh summary for all components.

Part	Element type	Average element size	Number of elements	Number of nodes
Bone cement	C3D8	0.5mm	12632	18891
Glenoid component	C3D8	0.5mm	68204	75081
Glenoid central peg	C3D10	0.5mm	15077	23061
Scapula	C3D10	1mm and 2mm	349578	520678
Total assembly	-	-	445491	637679

Loading conditions

The loads were retrieved from the musculoskeletal model of the upper limb developed by Quental et. al. [9]. This model includes 7 rigid bodies, 6 anatomical joints and 21 muscles. The GH joint is modelled as a spherical joint with clearance, allowing for the simulation of its 6 degrees of freedom.. In this study, abduction and flexion motions previously acquired at the Laboratory of Biomechanics of Lisbon were analyzed.

In the musculoskeletal model, the elastic force developed in the GH contact is described by a Hertz contact force model given by:

$$\begin{cases} F_N = 0, & \delta < 0 \\ F_N = K\delta^{1.5}, & \delta \geq 0 \end{cases} \quad (2.3)$$

where K is the generalized stiffness constant and δ is the relative normal deformation between the articular surfaces. The generalized stiffness was defined as

$$K = \frac{4}{3(\sigma_i + \sigma_j)}\sqrt{\frac{R_i R_j}{R_i + R_j}} \quad (2.4)$$

where R_i and R_j are the radii of the articular surfaces, and σ_i and σ_j are given by:

$$\sigma_k = \frac{1-{\nu_k}^2}{E_k}, (k = i, j). \quad (2.5)$$

In Equation (2.5), E_k is the elastic modulus of the material of component k and υ_k is its Poisson's ratio [16]. For the glenoid component, $E = 500MPa$ and a $\nu = 0.4$ were used, corresponding to UHMWPE, while for the humeral head, made of a cobalt-chromium alloy, $E = 230GPa$ and a $\nu = 0.3$, were used [14]. Overall, six load conditions were applied to each of the different TSA models. For the abduction movement, elevation angles of 30º, 70º and 110º were considered, while for the flexion movements, elevation angles of 30º, 80º and 105º were included.

Interaction properties and boundary conditions

The interactions bone-cement and cement-implant were bonded using tie constraints [17]. The interaction between the humeral head and glenoid component was modeled using a surface-to-surface contact formulation with a friction coefficient of 0.07 [17]. An automatic stabilization with a factor of 0.1 was also used to ensure model convergence.

To complete the finite element model, a boundary condition was defined to eliminate rigid body motion. To fix the scapula, an encastre condition was defined at the rhomboid muscle insertion [8].

2.3. Analysis of the FE results

The processing of the data retrieved from the finite element analyses was done with the goal of understanding the influence of GH conformity on the glenoid loosening mechanisms. The data gathered included Von Mises stresses for all nodes of the cement mantle and normal and shear stresses for all nodes of the bone-cement interface, which is considered the main area of glenoid loosening [8]. The Von Mises stresses in the bone cement were used to assess possible cement failure through fracture or crack generation, and the normal and shear stresses at the bone-cement interface were used

to compute the Hoffman failure criterion and determine the risk of failure of the interface.

Evaluation of the cement stresses

The Von Mises stresses of the cement mantle were retrieved for all nodes of the cement in all loading scenarios. These values were processed and the maximum value for each node was recorded. According to the literature, PMMA failure and crack initiation starts at 5 MPa [18]. Therefore, the stresses were compared to the failure stress of the cement in order to understand the percentage of nodes at risk of cement failure.

Hoffman Criterion

The Hoffman criterion is a quadratic formulation that evaluates the fixation of the interface between two components. This criterion uses both normal (σ_n) and shear stresses (τ) at the interface to determine if mechanical failure may occur, by assigning to each node an Hoffman number (H) that quantifies the risk of failure of that node. According to the criterion, if H is higher than 1, failure is expected to occur, whereas if H is lower than 1, no failure is expected. The Hoffman number is determined by [15]:

$$H = \frac{1}{S_t S_c}\sigma_n^2 + \left(\frac{1}{S_t} - \frac{1}{S_c}\right)\sigma_n + \frac{1}{S_s^2}\tau^2 \quad (2.6)$$

$$S_t = 14.5\rho^{1.71} \quad (2.7)$$

$$S_c = 32.4\rho^{1.85} \quad (2.8)$$

$$S_s = 21.6\rho^{1.65} \quad (2.9)$$

where S_t and S_c are the uniaxial interface tensile and compressive strengths, respectively, and S_s is the interface shear strength. The interface strengths depend on the bone density ρ of each node. This formulation was applied to all bone nodes from the bone-cement interface, for all load cases and different TSA configurations. To represent the worst possible scenario for each node, the highest Hoffman number among those calculated for the different load cases was selected for each node

3. Results

The results of this study are divided into three sections, the evaluation of glenohumeral translations, analysis of the contact pressures on the glenoid implant, analysis of the stresses on the cement mantle and the evaluation of the bone-cement interface through the application of the Hoffman criterion.

Glenohumeral translations

The evaluation of the results from the multibody model have shown that the reaction forces for the abduction movements were larger than those for the flexion movement. Besides, the glenohumeral conformity didn't seem to have significant influence on the magnitude of the reaction forces.

Moreover, the model showed that a less conforming design allows for wider humeral translations.

Finite element analysis

The evaluation of the contact pressures on the glenoid have shown that the contact area between the glenoid and humeral components decreases with increasing mismatch. This was translated into higher contact pressures in less conforming designs.

Analysis of the cement mantle stresses

The analysis of the von Mises stresses on the cement have shown that all configurations, and for the most part of the loading conditions (excluding 30º arm elevation for both flexion and abduction), present regions surpassing the 5 MPa threshold that indicates potential failure. The region with the highest risk of failure during abduction was the most anterior area, while during flexion it was the central area and the one surrounding the superior pin of the glenoid implant. For the sake of briefness only the results for 80º flexion are presented in Figure 3.1 as they are illustrative of the rest.

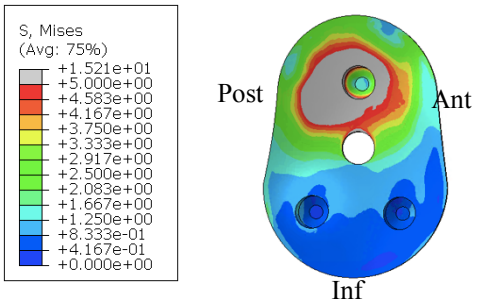

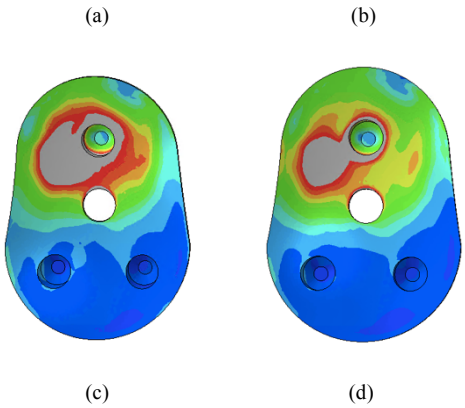

Figure 3.1: Von Mises stress distribution on the cement mantle for 80° flexion for (b) 5mm mismatch; (c) 3mm mismatch and (d) 1mm mismatch.

Figure 3.2 presents the cumulative percentage of nodes that are subjected to a specific Von Mises stress or higher, for each of the three articular configurations. The vertical red line corresponds to the stress over which fatigue failure of the PMMA can occur (5 MPa [19]). In the 1mm radial mismatch configuration, the percentage of elements at risk is lower than that of other configurations. The most conforming implant resulted in a percentage of cement at risk of 23%, which increased to 27% and 28% with increasing radial mismatch. However, at 7MPa, the difference between mismatches is larger, as the percentages at risk for 1mm, 3mm and 5mm were 7%, 15% and 16% respectively.

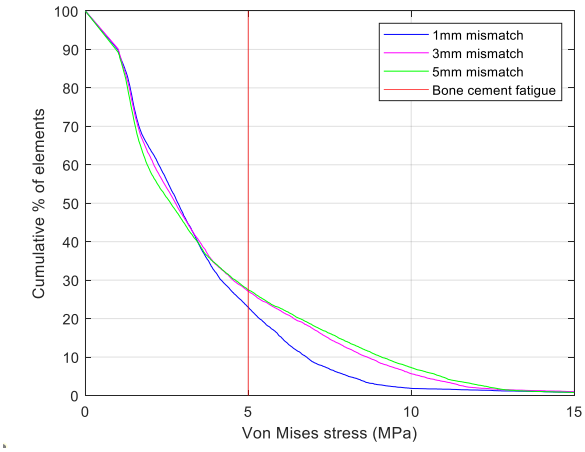

Figure 3.2: Cumulative percentage of nodes that are under specific Von Mises stress or higher.

Hoffman failure criteria

The distribution of the Hoffman numbers along the surface of the scapula connected to the PMMA is depicted in Figure 3.3 for the three configurations under study. The areas in gray represent those that are at risk of failure according to this criteria.

The anterior region presented an Hoffman number higher than 1 regardless of the conformity of the joint. As the radial mismatch increased, the Hoffman number also increased on the region of the upper peg. For the largest radial mismatch, the superior peg presents Hoffman numbers larger than 1, which was not observed for the remaining configurations. The areas in black correspond to negative Hoffman numbers.

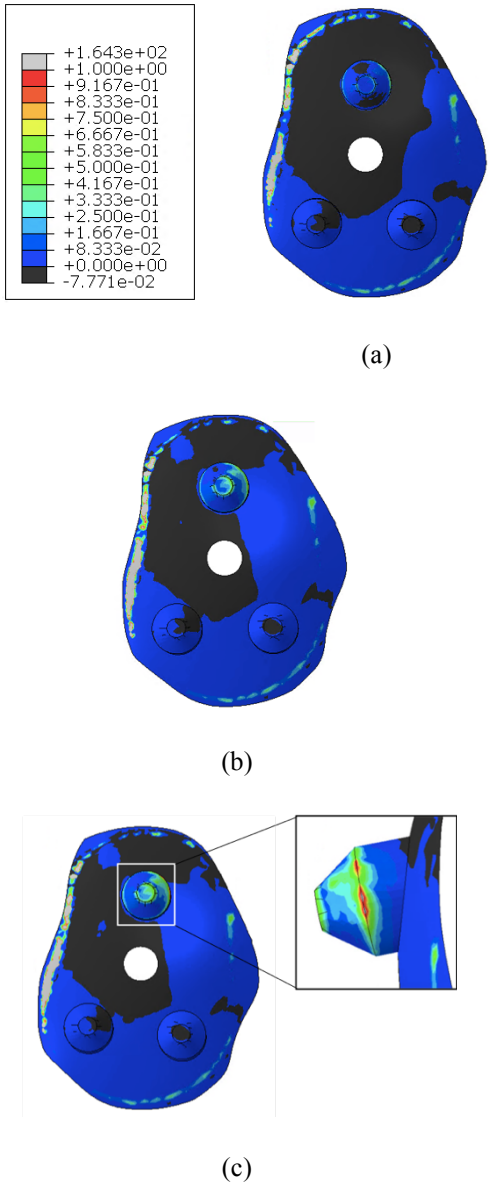

Figure 3.3: Hoffman number distributions for (a) 1mm mismatch; (b) 3mm mismatch and (c) 5mm mismatch.

Figure 3.4 presents the percentage of nodes of the bone-cement interface that are above a certain

Hoffman number, between 0 and 1, for the different conformities. The cumulative percentage of nodes with Hoffman number above zero does not start at 100% because some of the Hoffman numbers were negative, and, for the ease of the analyses, these numbers were neglected from the plot. The results show that most nodes had low Hoffman numbers, and that for high Hoffman numbers the difference between radial mismatches seemed negligible.

Post

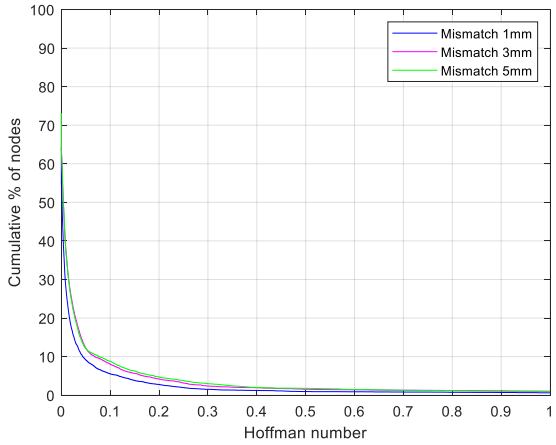

Figure 3.4: Cumulative percentage of nodes with Hoffman number between 0 and 1.

4. Discussion

This study aimed to evaluate the influence of the articular conformity in the mechanisms of glenoid loosening after an anatomic total shoulder arthroplasty. The three configurations analyzed had radial mismatches of 1mm, 3mm and 5mm and were subjected to six loading conditions each (abduction and flexion movements in three arm positions), which were obtained through the application of a musculoskeletal model of the upper limb [9].

Regarding the joint reaction forces at the GH joint, no relevant differences were observed in the magnitudes between different radial mismatches, even though the force increased with joint conformity. These results are consistent with previous computational models, which observed no influence of the GH translations on the joint reaction forces [9].

The humeral translations estimated by the musculoskeletal model increased with decreasing conformity, which is consistent with the less restricted kinematics of the joint. These results are supported by the literature. In fact, Hopkins et. al. [20] conducted a 3D FE analysis and have shown that under conditions of simple compressive loading, the humeral translations depended linearly on glenohumeral conformity, the most conforming the joint, the least humeral translations were allowed.

Moreover, the increasing mismatch also resulted in a decrease in contact area between the humeral head and glenoid components, and thus in an increase in contact pressure. Once again, the results are consistent with previous studies that show that not only decreased conformity leads to smaller contact areas, but also that the contact area has critical influence on the stress levels. Studies have found that for small contact areas the contact stresses increase, as found in the present study [21], [22].

The mechanisms of glenoid loosening were analyzed through the potential failure of the bone cement and the bone-cement interface. The evaluation of Von Mises stresses in the bone cement suggested that glenoid loosening may be a result of fatigue failure of the cement mantle in all configurations, with emphasis on less conforming designs, as a high percentage of the cement was under stresses higher than 5 MPa, considered to be the fatigue strength of the PMMA [18]. This is consistent with the literature—Lacroix and Prendergast [18] found similar results for a keeled implant, concluding that more conforming designs lead to more moderate stresses on the cement mantle. Moreover, Terrier et. al. [23] have shown that the Von Mises stress increased around 200% as the mismatch increased from 1 to 15mm, which is in line with the increasing stress on the cement mantle for increasing mismatch seen in this study.

Additionally, note that this study considered loading cases of unloaded abduction and flexion movements. Under other daily activities, the cement mantle may be subjected to much higher stresses, supporting the concern of cement failure.

Nevertheless, the value for the cement fatigue strength is not clear in the literature, ranging from 4MPa to 15 MPa, depending on the number of cycles and on the study performed [24]. Therefore, this analysis may be different if a higher reference is taken into consideration. However, the 5 MPa reference was chosen since it has been used in similar studies [18], [25].

The analysis of bone-cement interface using the Hoffman criterion showed that failure can occur in all configurations on the anterior region of the bone-cement interface. This zone presented low bone

density, which is another important factor when evaluating glenoid loosening mechanisms. In the two most conforming configurations, the only zone of the interface that failed was the anterior boundary; however, for the highest radial mismatch, the area surrounding the superior peg was also failing according to the Hoffman criterion.

Using both criteria, glenoid loosening may begin through cement failure and bone-cement debonding. Besides, the probability of cement failure of high-conformity joints is lower than that of low articular conformity designs. To sum up, for all radial mismatches studied, the configuration with highest conformity showed the lowest risk of failure, while the other two configurations showed similar results, with a difference in the evaluation of bone-cement detachment, where the 5mm mismatch design performed worse.

The findings of this study must be evaluated considering its limitations. Firstly, the loading scenarios were limited since a wide range of movements are performed every day. Daily living activities may be better suited for identifying different failure mechanisms of glenoid loosening. Secondly, the analysis was performed considering one specific shoulder joint anatomy, thus, the results may not be generalized for all glenohumeral joint.

Moreover, the evaluation of the distribution of stresses on the cement mantle considered the fatigue strength of the material and crack generation under cyclic loading, even though only static analyses were performed in this study. Besides, as mentioned before, there is no consensus in the literature regarding the failure strength of the cement.

The bone-cement and cement-implant interactions were assumed bonded, which does not allow for micromotion evaluation, as analyzed in some studies [14]. The evaluation of the micromotions would allow for the analysis of the implant-cement interface. Even though this is not considered to be the most relevant interface when studying glenoid loosening mechanisms, it would be interesting to evaluate and confirm whether the radial mismatch influences the interface failure.

Finally, the influence of bone density in all the evaluation criteria may have conditioned the results since a low-density region existed in the superior region of the reamed glenoid cavity.

5. Conclusions

The translations of the humeral head retrieved from the multibody model have shown that larger radial mismatches allow for greater humeral translations.

The stress distribution of the cement showed that fatigue failure and crack initiation is in the spectrum of possible complications since in all configurations stresses surpassed the endurance limit of the PMMA.

The Hoffman criterion analysis suggested two zones of possible detachment between the cement and bone, namely the superior peg and the regions with low bone density. Overall, the results suggested that the more conforming configuration has lower risks of failure under normal and healthy physiological conditions when compared to less conforming designs. However, the more conforming joint is still at risk of failure through both mechanisms identified.

Acknowledgement

This document was written and made publically available as an institutional academic requirement and as a part of the evaluation of the MSc thesis in Biomedical Engineering of the author at Instituto Superior Técnico. The work described herein was performed at Instituto Superior Técnico (Lisbon, Portugal), during the period March-October 2021, under the supervision of Prof. João Folgado and Prof. Carlos Quental.

References.

[1] K. I. Bohsali, A. J. Bois, and M. A. Wirth, “Complications of Shoulder Arthroplasty,” *Copyr. Ó 2017 BY J. BONE Jt. Surg.*, vol. 99, pp. 256–69, 2017, doi: 10.2106/JBJS.16.00935.

[2] B. BP, P. IM, C. B, T. RM, S. KL, and M. FA, “Patient functional self-assessment in late glenoid component failure at three to eleven years after total shoulder arthroplasty,” *J. shoulder Elb. Surg.*, vol. 14, no. 4, pp. 368–374, Jul. 2005, doi: 10.1016/J.JSE.2004.10.008.

[3] B. KI, W. MA, and R. CA, “Complications of total shoulder arthroplasty,” *J. Bone Joint Surg. Am.*, vol. 88, no. 10, pp. 135–141, 2006, doi: 10.2106/JBJS.F.00125.

[4] F. AK, L. TR, M. D, N. B, and M. FA, “The complex characteristics of 282

unsatisfactory shoulder arthroplasties," *J. shoulder Elb. Surg.*, vol. 16, no. 5, pp. 555–562, Sep. 2007, doi: 10.1016/J.JSE.2006.11.004.

[5] M. FA, B. RT, and L. SB, "Shoulder arthroplasty: the socket perspective," *J. shoulder Elb. Surg.*, vol. 16, no. 5 Suppl, Sep. 2007, doi: 10.1016/J.JSE.2007.02.112.

[6] S. B. Gunther, J. Graham, T. R. Norris, M. D. Ries, and L. Pruitt, "Retrieved glenoid components: A classification system for surface damage analysis," *J. Arthroplasty*, vol. 17, no. 1, pp. 95–100, 2002, doi: 10.1054/ARTH.2002.27671.

[7] B. JP, F. A, B. R, and M. FA, "Alterations in surface geometry in retrieved polyethylene glenoid component," *J. Orthop. Res.*, vol. 24, no. 6, pp. 1249–1260, Jun. 2006, doi: 10.1002/JOR.20158.

[8] C. Quental, P. R. Fernandes, J. Monteiro, and J. Folgado, "Bone remodelling of the scapula after a total shoulder arthroplasty," *Biomech. Model. Mechanobiol. 2013 134*, vol. 13, no. 4, pp. 827–838, Oct. 2013, doi: 10.1007/S10237-013-0537-5.

[9] Q. C, F. J, A. J, and M. J, "A new shoulder model with a biologically inspired glenohumeral joint," *Med. Eng. Phys.*, vol. 38, no. 9, pp. 969–977, Sep. 2016, doi: 10.1016/J.MEDENGPHY.2016.06.012.

[10] S. VJ, L. DJL, W. JD, P. V, and Z. L, "The effect of glenohumeral radial mismatch on different augmented total shoulder arthroplasty glenoid designs: a finite element analysis," *J. shoulder Elb. Surg.*, vol. 28, no. 6, pp. 1146–1153, Jun. 2019, doi: 10.1016/J.JSE.2018.11.059.

[11] Integra LifeSciences, "TITAN Modular Shoulder System," 2013. [Online]. Available: http://integralife.com/index.aspx?redir=detailproduct&Product=735&ProductName=TITAN Modular Shoulder System&ProductLineName=Shoulder & Elbow&ProductLineID=72&PA=Upper Extremity.

[12] DePuy Synthes, "GLOBAL^{TM} APG Anchor Peg Glenoid Shoulder System Surgical Technique."

[13] DePuy Synthes, "Global AP Surgical technique."

[14] W. Pomwenger, K. Entacher, H. Resch, and P. Schuller-Götzburg, "Influence of glenoid implant depth on the bone–polymethylmethacrylate interface," *Obere Extrem. 2019 144*, vol. 14, no. 4, pp. 284–291, Mar. 2019, doi: 10.1007/S11678-019-0512-6.

[15] G. S, van der H. FC, and van K. F, "The possibilities of uncemented glenoid component--a finite element study," *Clin. Biomech. (Bristol, Avon)*, vol. 19, no. 3, pp. 292–302, Mar. 2004, doi: 10.1016/J.CLINBIOMECH.2003.12.002.

[16] M. Machado *et al.*, "Development of a planar multibody model of the human knee joint," *Nonlinear Dyn.*, vol. 60, no. 3, pp. 459–478, May 2010, doi: 10.1007/S11071-009-9608-7.

[17] J. Zhang *et al.*, "Glenoid articular conformity affects stress distributions in total shoulder arthroplasty," *J. Shoulder Elb. Surg.*, vol. 22, no. 3, pp. 350–356, Mar. 2013, doi: 10.1016/J.JSE.2012.08.025.

[18] L. D and P. PJ, "Stress analysis of glenoid component designs for shoulder arthroplasty," *Proc. Inst. Mech. Eng. H.*, vol. 211, no. 6, pp. 467–474, 1997, doi: 10.1243/0954411981534583.

[19] D. JP, B. DW, O. DO, and H. WH, "Comparison of the fatigue characteristics of centrifuged and uncentrifuged Simplex P bone cement," *J. Orthop. Res.*, vol. 5, no. 3, pp. 366–371, 1987, doi: 10.1002/JOR.1100050308.

[20] H. Andrew R, H. Ulrich N, A. Andrew A, T. Mark, and E. Roger J, "Glenohumeral kinematics following total shoulder arthroplasty: a finite element investigation," *J. Orthop. Res.*, vol. 25, no. 1, pp. 108–115, Jan. 2007, doi: 10.1002/JOR.20290.

[21] W. G, E. TB, B. A, B. P, M. D, and A. P, "The influence of glenohumeral prosthetic mismatch on glenoid radiolucent lines: results of a multicenter study," *J. Bone Joint Surg. Am.*, vol. 84, no. 12, pp. 2186–2191, Dec. 2002, doi: 10.2106/00004623-200212000-00010.

[22] C. B, M. P, E. E, D. R, M. M, and E. J, "Finite element analysis of the mechanical behavior of a scapula implanted with a glenoid prosthesis," *Clin. Biomech. (Bristol, Avon)*, vol. 16, no. 7, pp. 566–575, 2001, doi: 10.1016/S0268-0033(01)00029-8.

[23] A. Terrier, P. Büchler, and A. Farron, "Influence of glenohumeral conformity on glenoid stresses after total shoulder arthroplasty," 2006, doi: 10.1016/j.jse.2005.09.021.

[24] T. A, B. P, and F. A, “Bone-cement interface of the glenoid component: stress analysis for varying cement thickness,” *Clin. Biomech. (Bristol, Avon)*, vol. 20, no. 7, pp. 710–717, Aug. 2005, doi: 10.1016/J.CLINBIOMECH.2005.03.010.

[25] L. D, M. LA, and P. PJ, “Three-dimensional finite element analysis of glenoid replacement prostheses: a comparison of keeled and pegged anchorage systems,” *J. Biomech. Eng.*, vol. 122, no. 4, pp. 430–436, 2000, doi: 10.1115/1.1286318.